CrossMark

Application of thermal ignition theory of di(2,4-dichlorobenzoyl) peroxide by kinetic-based curve fitting

Chen-Rui Cao[1] · Shang-Hao Liu[2] · An-Chi Huang[1] · Ming-Hsun Lee[1] · San-Ping Ho[4] · Wen-Lung Yu[1,3] · Chi-Min Shu[1,5]

Abstract

Di(2,4-dichlorobenzoyl) peroxide (DCBP), classified as a diacyl peroxide, is commonly used in silicone rubber manufacturing as a crosslinking agent, vulcanizing agent, and polymerization initiator. However, its reactivity or incompatibility may negatively affect safety requirements and concerns during chemical reactions. This study was conducted to investigate the properties of DCBP by using differential scanning calorimetry and a literature review. Specifically, thermal decomposition behavior of DCBP was examined by combining simulations with thermal analysis methods to analyze the foundation of thermokinetics, such as the peak temperature, heat of decomposition, and apparent activation energy of DCBP. Based on parameters obtained from the calculations, this investigation was integrated with thermal explosion theory, which represents a major advancement in the comprehension of behavior between heat release and heat transfer to the surroundings incorporated into a single differential equation, and a decision was made from a criticality criterion simultaneously.

Keywords Di(2,4-dichlorobenzoyl) peroxide (DCBP) · Polymerization initiator · DSC · Thermal decomposition · Thermal analysis

List of symbols

A	Pre-exponential factor of Arrhenius equation, min^{-1}
$A(\alpha)$	Pre-exponential factor of Arrhenius equation at conversion α, min^{-1}
$A'(\alpha)$	Modified pre-exponential factor by a product of $A(\alpha)$ and $f(\alpha)$, min^{-1}
α	Reaction conversion, dimensionless
β	Heating rate, $°C\ \text{min}^{-1}$
C_o	Initial concentration of the reaction, g cm^{-3}
C	Concentration of the reaction, g cm^{-3}
C_p	Specific heat of material, $\text{J g}^{-1}\ \text{K}^{-1}$
E_a	Apparent activation energy, kJ mol^{-1}
$E(\alpha)$	Apparent activation energy at conversion α, kJ mol^{-1}
$f(\alpha)$	Reaction equation, dimensionless
h	Heat exchange capability index of the cooling system, $\text{kJ m}^{-2}\ \text{K}^{-1}\text{min}^{-1}$
k	Reaction rate constant, dimensionless
n	Reaction order, dimensionless
m	Mass of material, g
ΔH_d	Heat of decomposition, J g^{-1}
ΔH_t	Heat of decomposition at t, J g^{-1}
ΔH_{total}	Heat of decomposition from material, J g^{-1}
Q_g	Heat production rate, kJ min^{-1}
Q_r	Heat discharge rate, kJ min^{-1}

✉ Shang-Hao Liu
shliu998@163.com

✉ Chi-Min Shu
shucm@yuntech.edu.tw

1 Graduate School of Engineering Science and Technology, National Yunlin University of Science and Technology (YunTech), Yunlin 64002, Taiwan, ROC

2 Department of Ammunition Engineering and Explosion Technology, Anhui University of Science and Technology, Anhui 232001, China

3 Department of Industrial Education and Technology, National Changhua University of Education, Changhua 50074, Taiwan, ROC

4 Department of Occupational Safety and Health, Chang Jung Christian University, Tainan 71101, Taiwan, ROC

5 Department and Graduate School of Safety, Health, and Environmental Engineering, Center for Process Safety and Industrial Disaster Prevention, YunTech, Yunlin 64002, Taiwan, ROC

Q_{r1} Heat discharge rate by high cooling medium, kJ min^{-1}

Q_{r2} Heat discharge rate by cooling system, kJ min^{-1}

Q_{r3} Heat discharge rate by low cooling system, kJ min^{-1}

Q_{max} Maximum heat discharge rate, kJ min^{-1}

R Gas constant, 8.31415 J K^{-1} mol^{-1}

R^2 Coefficient of determination, dimensionless

r Reaction rate, mol L^{-1} s^{-1}

S Effective heat exchange area, m^2

T Process temperature, K

T_0 Apparent exothermic temperature, K

T_a Surrounding temperature under cooling system, K

$T_{C,I}$ Critical ignition temperature, K

$T_{C,E}$ Critical extinguished temperature, K

T_{max} Temperature at the maximum heat release in reaction, K

T_M Cutoff point between curves Q_g and Q_r at the highest and lowest cooling efficient system, K

$T_{S,E}$ Stable point of extinguished temperature, K

$T_{S,I}$ Stable point of ignition temperature, K

$T_{S,L}$ Stable point at low temperature, K

$T_{S,H}$ Stable point at high temperature, K

t Reaction time, min

V Volume of process instrument, m^3

X_A Fractional conversion, dimensionless

Introduction

Forecasts on the demand for organic peroxides (OPs) in the global market indicate gradual growth, especially in the Asia–Pacific region. The value of which is predicted to reach US$ 2.1 billion between 2015 and 2020 [1]. Diacyl OPs, such as dibenzoyl peroxide, di(2,4-dichlorobenzoyl) peroxide (DCBP), and dicumyl peroxide are commonly used as radical initiators or catalysts in polymerization or crosslinked reactions [2–4]. Most OPs are typically activeness and instability which can act as a heat source provided in the polymerization reaction. However, they also have been reported to incur thermal damage or induce runaway reactions or explosions during chemical reaction processes or in oxidation vessels or reactors [5–7]. According to the nine classes of hazardous materials by the Federal Motor Carrier Safety Administration of the United States Department of Transportation (U.S. DOT), OPs are classified into Division 5.2 in Class 5 of hazardous materials [8]. Hence, safety concerns about OPs must be paramount in chemical plants, including transportation, and storage. DCBP 50.0 mass% in silicone oil is a common commercial product. DCBP is essentially a solid that is insoluble in water and slightly unstable to reducing agents,

acids, and alkalis [9–11]. DCBP is assigned into type D of OPs following the Globally Harmonized System of Classification and Labelling of Chemicals UN [12].

A literature review indicated that the thermal hazards of OPs have been studied, such as benzoyl peroxide, cumene hydroxide, 1,1-bis (tert-butylperoxy) cyclohexane, lauroyl peroxide, and methyl ethyl ketone peroxide [6, 7, 13–17]. However, little research exists on DCBP. Therefore, our main objective was to evaluate the thermal hazard of DCBP. Differential scanning calorimetry (DSC) was employed to record thermal decomposition parameters, such as exothermic onset temperature (T_0), exothermic peak temperature (T_{max}), and heat of decomposition or enthalpy (ΔH_d). We evaluated the thermal decomposition kinetic of the apparent activation energy (E_a) using a reaction model [18–22]. Numerical simulation methods are often used in kinetic evaluations from calorimetric data, and they provide an appropriate fit [5, 13, 16, 23–27]. Therefore, the curve fitting simulation method was applied in this study for kinetic evaluation and to obtain the thermal stability kinetic parameters of DCBP. The simulation involved three major steps for the construction of a kinetic model of a test sample or an object. First, laboratory-scale thermal calorimetric experimental data were utilized. Second, a proper reaction kinetic model was chosen based on previous experimental data. Finally, the kinetic model was incorporated into the model of an object and the behavior of the test sample was predicted from the simulation results, as suggested by Kossoy [28, 29].

Experimental

Samples

DCBP of 50.0 mass% dissolved in silicone oil solvent in paste form (CAS no. 133–14–2, $C_{14}H_6Cl_4O_4$), other 50.0 mass% component was poly(dimethylsiloxane), an inert, nontoxic, nonflammable compound which is most widely used in silicon-based organic polymer materials. DCBP, which is white to slightly yellow with faint aromatic odor, was purchased from Aceox$^®$ Chemical Corp. (Taoyuan, Taiwan, ROC) [30]. To avert a hot external environment and maintain stability, it was stored in a refrigerator at 8.0 °C.

Differential scanning calorimetry

DSC coupled with STAR^e software (DSC821^e Mettler TA8000 system) was applied to measure the heat flow difference between a sample and a reference, both set on different pans but in the same furnace [31]. A high-pressure gold-plated steel seal-tightened crucible was used to resist the evaporation of the peroxide during scanning. To

approach thermal equilibrium, heating rates (β) were set at 0.5, 1.0, 2.0, 4.0, and 8.0 °C min^{-1}, respectively. The rising temperature range was from 30.0 to 200.0 °C, and the material mass was set from 3.0 to 5.0 mg. The change in heat flow versus sample temperature was obtained through DSC testing, and then T_0, T_{max}, and ΔH_d were calculated using STAR^e.

Results and discussion

Thermokinetic parameters from calorimetric data

The thermal decomposition parameters from DSC are presented in Table 1. As illustrated in Fig. 1, the decomposition of DCBP through DSC at each heating rate showed one obvious exothermic curve; however, curves at heating rates of 0.5, 1.0, 2.0, 4.0, and 8.0 °C min^{-1} demonstrated a swift reduction in the heat release rate as the temperature (or time) increased, unlike the typical thermal curves of dynamic DSC experiments [5, 32]. To compare tests, the ratios of maximum exothermic heat flow from the highest (22.77 W g^{-1}, 8.0 °C min^{-1}) to the lowest (1.53 W g^{-1}, 0.5 °C min^{-1}) were tested 15 times. The results showed that DCBP releases high exothermic heat when under high-temperature conditions or high heat is supplied from the environment.

Isoconversional differential using the Friedman method and Flynn–Wall–Ozawa method to obtain the basic thermal hazard parameters

For simulating for large-scale condition, we used the nonlinear fitting equations as Friedman method and Flynn–Wall–Ozawa method to determine E_a [22] combined with curve fitting equation as Kissinger method, which was also used in this study for calculating A to provide the correct kinetic parameters of DCBP.

Thermokinetic model is usually considered a particular reaction model function [24], assuming it represents the dependence of the conversion on the reaction rate. For example, the basic thermal parameter E_a in the Arrhenius equation is frequently described as a constant. Yet, the form of the decomposition reaction is generally intricate;
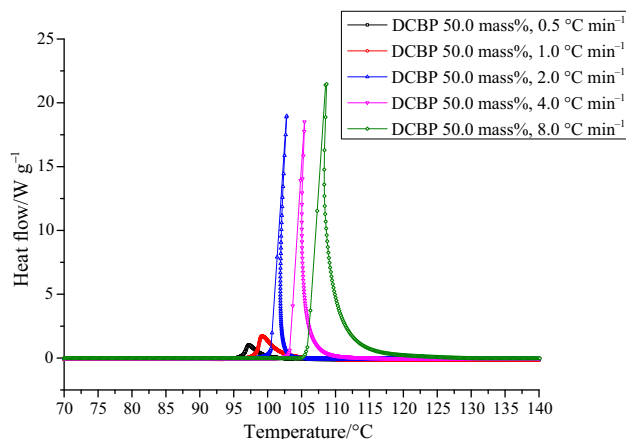

Fig. 1 Thermal curves of heat flow versus temperature on DCBP 50.0 mass% at five different heating rates (β = 0.5, 1.0, 2.0, 4.0, 8.0 °C min^{-1}) by DSC

therefore, the E_a and reaction mechanism might be altered with time or temperature. This means that E_a is a variable that is modified with the progress of the reaction instead of a constant. E_a is usually presented as a constant in the Arrhenius equation [26]. Nevertheless, decomposition reactions forms are often complicated; therefore, E_a and the decomposition mechanism may change with time or temperature. Thus, E_a may not be a constant value but a variable depending on the reaction form. However, the mode of reaction is not necessary in the isoconversional method.

The isoconversional method requires several kinetic curves at different temperature programs to perform the analysis [27]. The data can be calculated by taking the natural logarithm of the conversion rate formula (da/dt), externalized into absolute temperature inverse of the reaction conversion (α) [22]:

$$\ln\left(\frac{d\alpha}{dt}\right) = \ln(A(\alpha)f(\alpha)) \exp\left(-\frac{E(\alpha)}{RT(t)}\right) \tag{1}$$

$$t_a = \int_0^t dt = \int_{\alpha_0}^{\alpha} \frac{d\alpha}{A\prime(\alpha) \exp\left(-\frac{E(\alpha)}{RT(t)}\right)} \tag{2}$$

In Eq. (1), $E(\alpha)$ and $A(\alpha)$ represent apparent activation energy and pre-exponential factors at conversion α, and $A'(\alpha)$ denotes a value product from $A(\alpha)$ and $f(\alpha)$, which is

Table 1 Thermokinetic parameters of DCBP 50.0 mass% by DSC and comparisons on maximum heat flow between lower and high heating rates

β/ °C min^{-1}	Mass/mg	T_0/ °C	T_{max}/ °C	ΔH_d/J g^{-1}	Q_{max}/W g^{-1}
0.5	4.6	95.94	96.53	339.29	1.53
1.0	3.1	98.33	99.21	359.10	1.81
2.0	3.1	100.81	102.76	348.39	16.07
4.0	2.1	102.65	104.30	354.95	17.63
8.0	1.1	106.20	107.61	361.10	22.77

expressed as a variable exponential factor. $f(\alpha)$ is a reaction equation and has different expressions depending on the reaction form. However, this method is irrespective of the reaction form; therefore, $f(\alpha)$ can be can be set as a constant term. Negative $E(\alpha)/R$ and $\ln(A(\alpha)f(\alpha))$ can be represented as the slope and intercept, respectively. For coordinates, $\ln(d\alpha/dt)$ and $1/T(t)$ were plotted by the x-axis and y-axis, respectively.

Isoconversional integration using the Flynn–Wall–Ozawa method

The Flynn–Wall–Ozawa method inherits the advantages from the isoconversional model, which prevents the errors caused due to different assumptions on reaction forms. However, it is limited to the use of a linear variation of the temperature. Through Flynn–Wall–Ozawa method, a reaction form can be confirmed as follows [25]:

$$\ln(\beta) = -1.0516\frac{E_a}{RT} + \text{constant} \tag{3}$$

Kinetics data at several different heating rates can be expressed as:

$$\begin{aligned}
\ln(\beta_1) + 1.0516\frac{E_a}{RT_{\alpha 1}} &= \ln(\beta_2) + 1.0516\frac{E_a}{RT_{\alpha 2}} \\
&= \ln(\beta_3) + 1.0516\frac{E_a}{RT_{\alpha 3}} \\
&= \ln(\beta_4) + 1.0516\frac{E_a}{RT_{\alpha 4}} = \ldots
\end{aligned} \tag{4}$$

where β is the heating rate, E_a is the apparent activation energy, T is the process temperature, and R is the gas constant. The values of $\ln(\beta)$ relative to T^{-1} can be consequently used to acquire the slope as E_a in the plot.

Kinetic analysis using the curve fitting method (Kissinger method)

Recently, the general activation energy, temperature, or conversion are gradually no longer to be treated as a single variable, which can define as recombination of processes. However, the classical notion of obtaining a single number of apparent activation energy and pre-exponential factor exemplifying as process condition by a linear fitting method does not completely lose its attractiveness.

The relative rapidity and convenience for calculating required parameters are the advantages of the linear fitting method. The Kissinger method used in this study is based on the Arrhenius behavior, which requires four or more experiments at different heating rates, usually between 1 and 10 °C min^{-1} and assumes reaction as first-order kinetics. Basic thermal properties, such as decomposition crystallization, and degradation, are widely used to

estimate from this method [18–20]. The E_a and pre-exponential factor A can be determined by comparing the DSC data values on the y-axis ($\ln[\beta/T_p^2]$) with the linear relationship on the x-axis ($1/T_p$):

$$\ln\left(\frac{\beta}{T_p^2}\right) = \ln\left(\frac{AR}{E_a}\right) - \frac{E_a}{RT_p} \tag{5}$$

where A is the pre-exponential factor, β is the heating rate, E_a is the apparent activation energy, T is the reaction temperature, T_P is the absolute temperature at the maximum heat release in reaction, and R is the gas constant.

The simulation results using the three described methods are presented in Table 2 and Figs. 2–4. The values of the variation range of apparent activation energy in different reaction progress achieved from the Friedman method had the maximum numerical spacing than Flynn–Wall–Ozawa method. The single value of activation energy obtained by Kissinger method was closer to the range of Flynn–Wall–Ozawa. Here its coefficient of determination was 0.994. We selected the value calculated by Kissinger method as the basis for the subsequent simulation of the process amplification mode.

Scale-up and critical runaway parameter kinetic analysis

At the beginning of Semenov theory [33, 34], the temperature distribution in the reaction system is assumed to be unvarying, which is close on homogeneous system of the container. The heat generating efficiency of a substance in a container at a fixed volume (V) can be signified as Eq. (6):

$$Q_g = qV(-r_b) \tag{6}$$

where q is the exothermic heat of the reaction and $-r_b$ is its reaction rate. The rate of reaction represented by Arrhenius formal is replaced into Eq. (6), and heat generation can be acquired as Eq. (7):

$$Q_g = \Delta H_{\text{total}} V A C^n \exp\left(-\frac{E_a}{RT}\right) \tag{7}$$

Table 2 Comparison of kinetic parameters with isoconversional and curve fitting kinetic methods

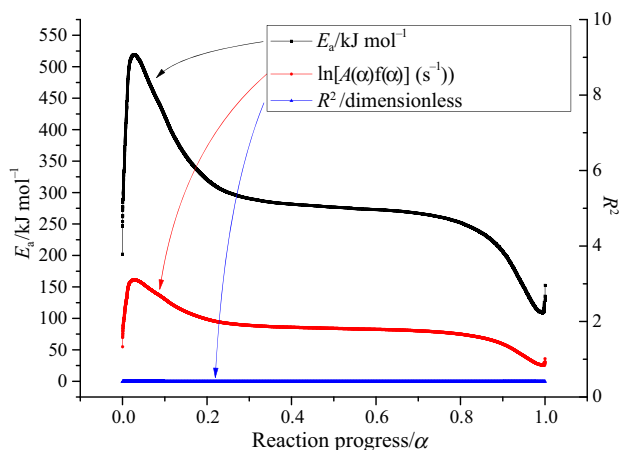| Method	Mathematical model	E_a/kJ mol^{-1}
Friedman	Isoconversional	120–500
Flynn–Wall–Ozawa	Isoconversional	140–280
Kissinger	Curve fitting	271

Fig. 2 Determination of the apparent activation energy of the decomposition of 50.0 mass% DCBP with the Friedman kinetic equation
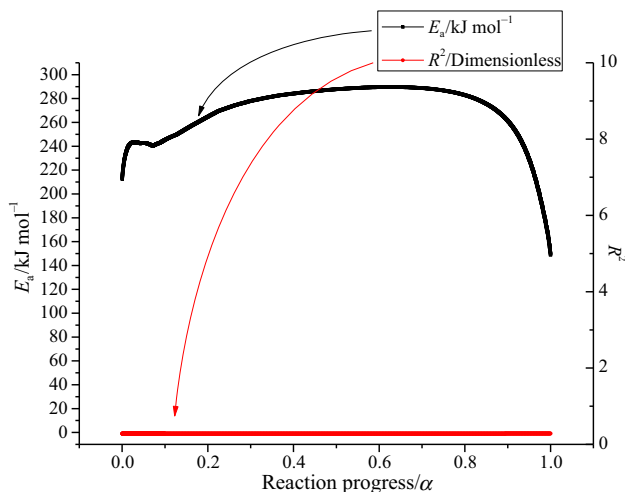

Fig. 3 Determination of the apparent activation energy of the decomposition of 50.0 mass% DCBP with the Flynn–Wall–Ozawa kinetic equation

The heat removal rate from the vessel to the ambient cooling medium is expressed as Eq. (8):

$$Q_r = hS(T - T_a) \tag{8}$$

where h is the convective heat transfer coefficient of the ambient medium, and S is the external surface area of the vessel. T and T_a are temperatures of the container and the cooling medium, respectively.

The heat balance within a fixed volume system can be found by subtracting heat removal from heat generation, as presented in Eq. (9):

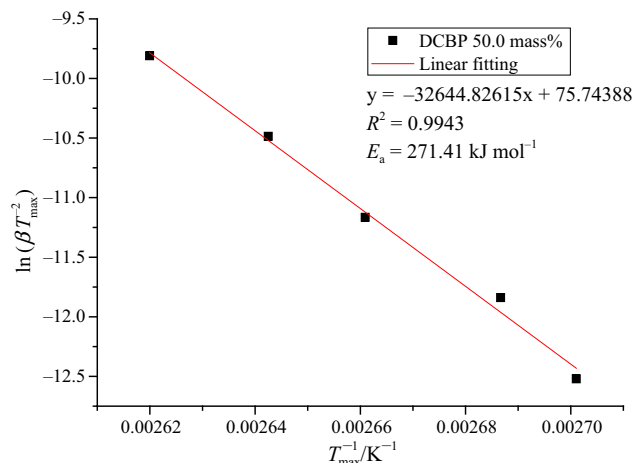$$\rho V C_P \left(\frac{dT}{dt}\right) = Q_g - Q_r \tag{9}$$

Fig. 4 Determination of the apparent activation energy of the decomposition of 50.0 mass% DCBP with the Kissinger method

The first term on the right indicates the exothermic heat from reaction, and the second term refers exothermic heat from system. The overall energy balance in Eqs. (7)–(9) can be represented as Eq. (10):

$$\rho V C_P \left(\frac{dT}{dt}\right) = \Delta H_{total} V A C^n \exp\left(-\frac{E_a}{RT}\right) - hS(T - T_a) \tag{10}$$

The reaction order, n, of the decomposition of DCPO is assumed to be unity. Thus, substituting Eq. (7) into Eq. (10) with $n = 1$ yields Eq. (11):

$$\rho V C_P \left(\frac{dT}{dt}\right) = \Delta H_{total} V A C_o \left[\frac{(T_p - T)}{(T_p - T_o)}\right] \exp\left(-\frac{E_a}{RT}\right) - hS(T - T_a) \tag{11}$$

when $(dT/dt) = 0$ means system in a steady-state situation, the necessary and sufficient conditions for satisfying the critical condition of the reaction system are expressed as Eqs. (12) and (13):

$$Q_g|_{T=T_c} = Q_r|_{T=T_c} \tag{12}$$

and

$$\left.\frac{dQ_g}{dT}\right|_{T=T_c} = \left.\frac{dQ_r}{dT}\right|_{T=T_c} \tag{13}$$

However, when $(dT/dt) > 0$, Q_g is greater than Q_r, may reflect the phenomenon of heat accumulation within the system, resulting in runaway reaction. Consequently, Eq. (11) can be rewritten as Eq. (14):

$$\Delta H_{total} V A C_o \left[\frac{(T_p - T_c)}{(T_p - T_o)}\right] \exp\left(-\frac{E_a}{RT_c}\right) = hS(T_c - T_a) \tag{14}$$

Fig. 5 Balance diagram of heat production rate q_g and heat removal rate q_r for decomposition reaction of 50.0 mass% DCBP with $T_a = 323.0$ K, $V = 50.0$ L
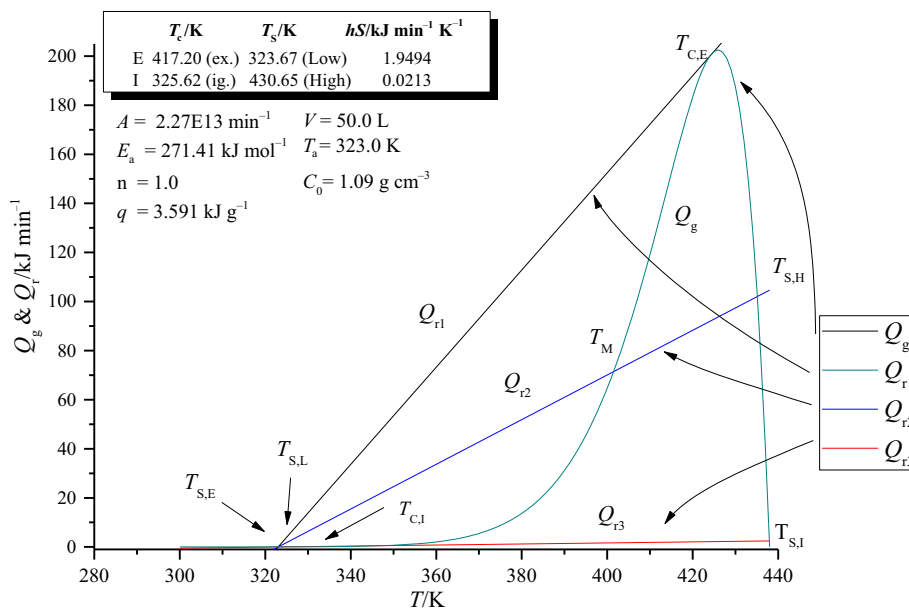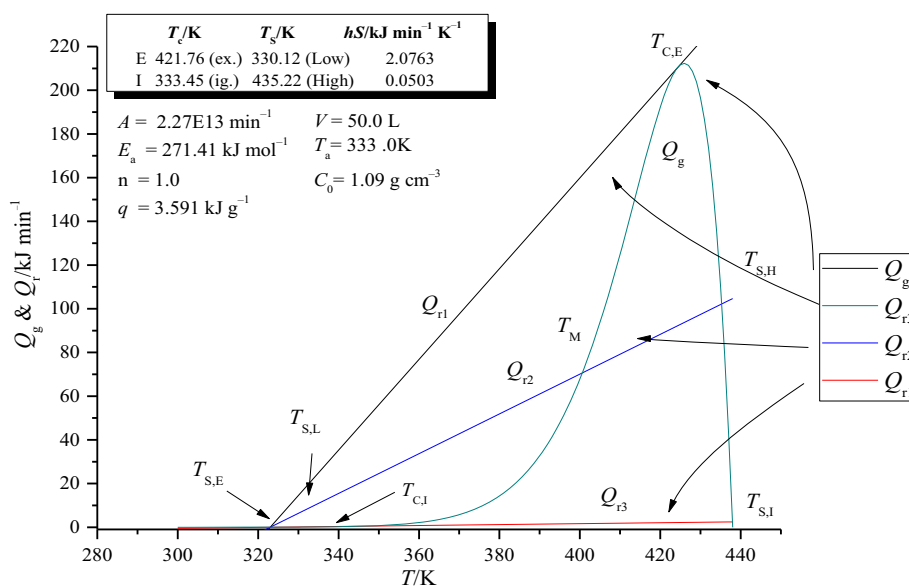

	T_c/K	T_s/K	hS/kJ min^{-1} K^{-1}
E	417.20 (ex.)	323.67 (Low)	1.9494
I	325.62 (ig.)	430.65 (High)	0.0213

$A = 2.27E13$ min^{-1} $V = 50.0$ L
$E_a = 271.41$ kJ mol^{-1} $T_a = 323.0$ K
n = 1.0 $C_0 = 1.09$ g cm^{-3}
$q = 3.591$ kJ g^{-1}

Fig. 6 Balance diagram of heat production rate q_g and heat removal rate q_r for decomposition reaction of 50.0 mass% DCBP with $T_a = 333.0$ K, $V = 50.0$ L

	T_c/K	T_s/K	hS/kJ min^{-1} K^{-1}
E	421.76 (ex.)	330.12 (Low)	2.0763
I	333.45 (ig.)	435.22 (High)	0.0503

$A = 2.27E13$ min^{-1} $V = 50.0$ L
$E_a = 271.41$ kJ mol^{-1} $T_a = 333.0$ K
n = 1.0 $C_0 = 1.09$ g cm^{-3}
$q = 3.591$ kJ g^{-1}

By taking into account, the conditions of Eqs. (12) and (14) are acquired as Eq. (15):

$$hS = \frac{\Delta H_{total} VAC_o \exp\left(-\frac{E_a}{RT_o}\right)\left[-1 + \frac{E_a(T_p - T_c)}{RT_c^2}\right]}{(T_p - T_o)} \quad (15)$$

In addition, Eq. (8) can be written as Eq. (16):

$$\Delta H_{total} VAC_o \left[\frac{(T_{max} - T_c)}{(T_{max} - T_o)}\right] \exp\left(-\frac{E_a}{RT_C}\right) = hS(T_c - T_a) \quad (16)$$

From Eq. (15) and (16), we can deduce the system's required heat removal efficiency hS.

The critical temperature, T_c, indicates that if the temperature in the system exceeds this value, runaway reactions will be occurring, critical temperature is jointly determined by the activation energy (E_a), temperature of the cooling system (T_a), and the maximum temperature when reaction has maximum heat generated (T_{max}).

Figures 5–10 show the results of calculating critical temperatures under different volumes (most of the packaging of standard containers is between $V = 25.0$ and 50.0 L) for the decomposition reaction of 50.0 mass% DCBP. T_a is set as 323.0, 333.0, and 343.0 K. Consider, for example, the result of $V = 50.0$ L. The two critical temperature values can be determined by the two points at

Fig. 7 Balance diagram of heat production rate q_g and heat removal rate q_r for decomposition reaction of 50.0 mass% DCBP with $T_a = 343.0$ K, $V = 50.0$ L
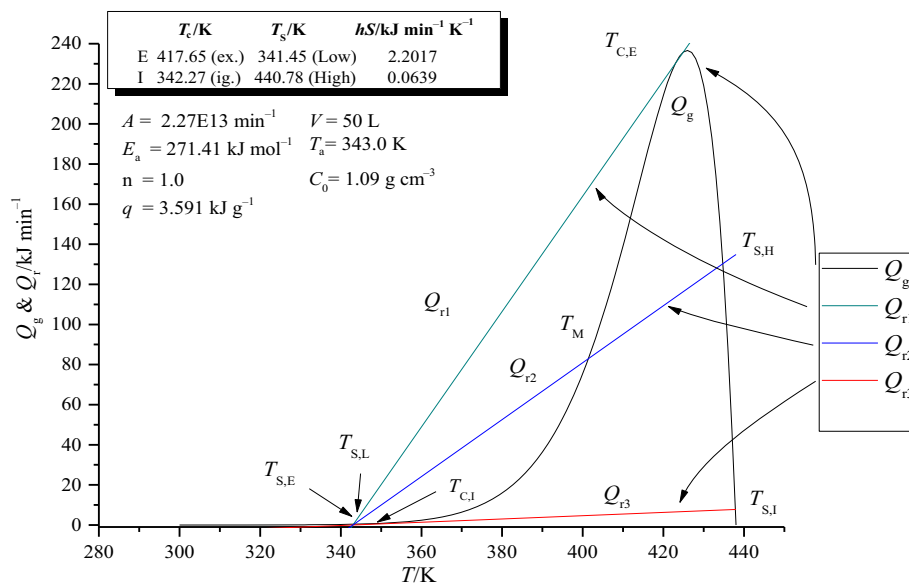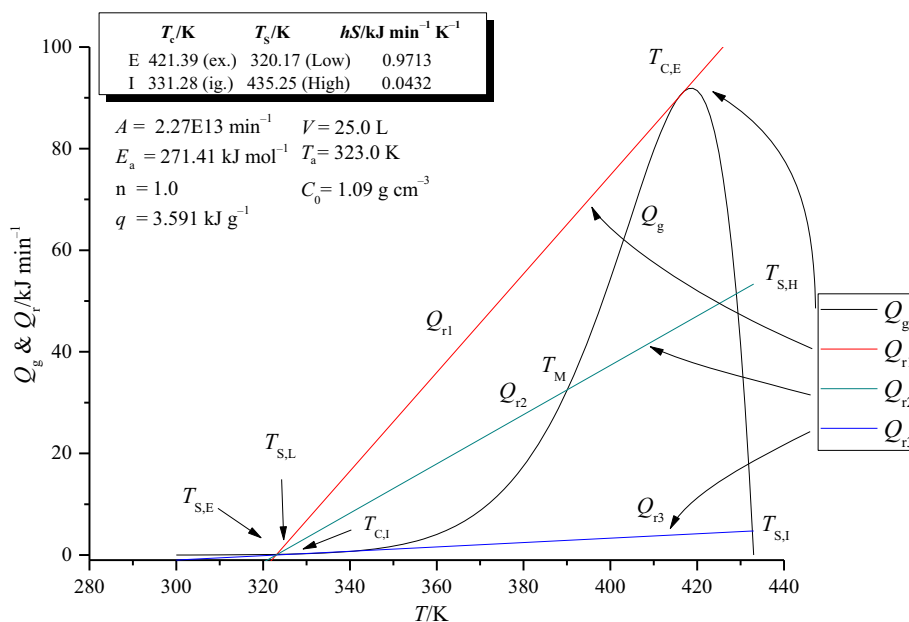

Fig. 8 Balance diagram of heat production rate q_g and heat removal rate q_r for decomposition reaction of 50.0 mass% DCBP with $T_a = 323.0$ K, $V = 25.0$ L

which the heat removal curve tangent and intersection to the heat generation curve, which express critical extinction temperature $T_{C,E}$ and critical ignition temperature $T_{C,I}$, respectively. Substituting the two values of T_c into Eq. (15) gives the hS value, which is the total heat transfer coefficient multiplied by the container's surface area. The values of hS can be derived into Eq. (16) and performing an iteration result in another set of temperatures, denoted as $T_{S,E}$ and $T_{S,I}$.

The following scenarios can be summarized by changes in temperature within the system, changes between heat removal and heat generation, and different cooling efficiencies. For low cooling efficiency of the system, $T_{C,E}$ and

$T_{C,I}$ are the intersection points between the line of heat removal (Q_{r3}) and the heat generated curve (Q_g), respectively, Consequently, if the system temperature exceeds $T_{C,I}$, at the same time $Q_{r1} < Q_g$. The reaction system leads into runaway condition and the temperature is gradually increased to reach $T_{C,E}$. However, even if the process reaction continues to cause the temperature to exceed $T_{C,E}$, then the $Q_{r3} > Q_g$, and the temperature will return to $T_{C,E}$.

For high cooling efficiency of the system, $T_{S,E}$ and $T_{S,I}$ are the intersection points between the line of heat removal (Q_{r1}) and the heat generated curve (Q_g); for this situation, the heat removal is often higher than the heat generation,

Fig. 9 Balance diagram of heat production rate q_g and heat removal rate q_r for decomposition reaction of 50.0 mass% DCBP with $T_a = 333.0$ K, $V = 25.0$ L
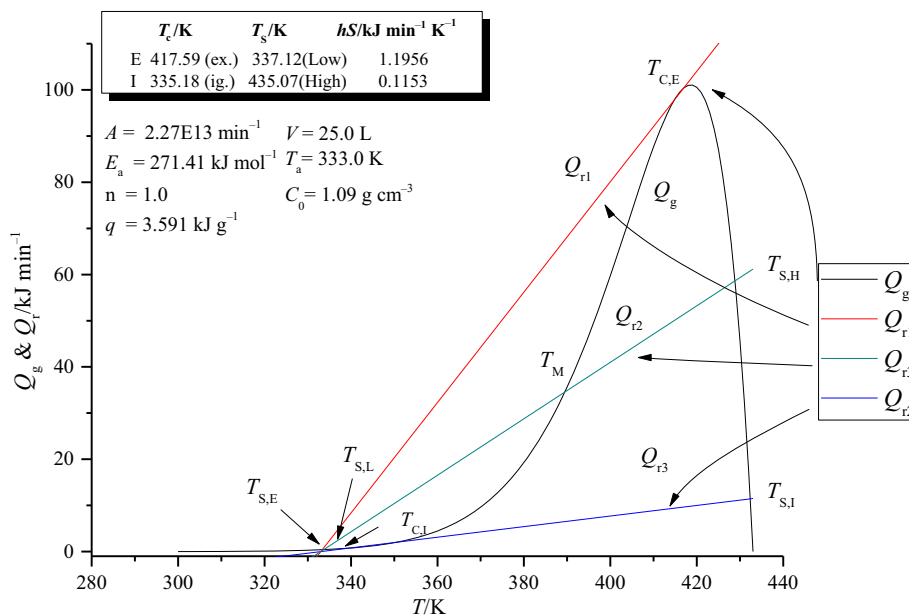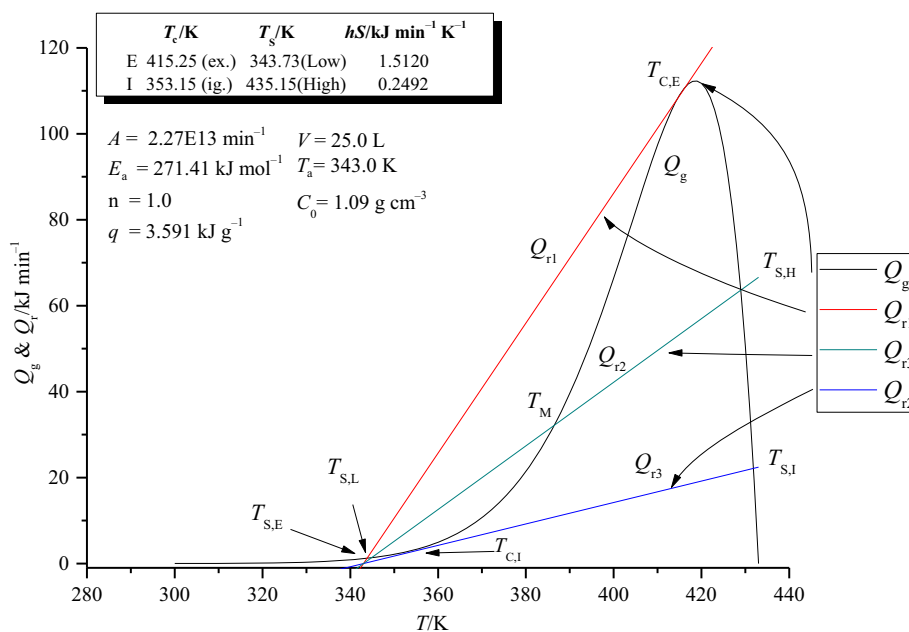

Fig. 10 Balance diagram of heat production rate q_g and heat removal rate q_r for decomposition reaction of 50.0 mass% DCBP with $T_a = 343.0$ K, $V = 25.0$ L

and even when the temperature exceeds the value of $T_{S,I}$, system still does not produce runaway phenomenon.

For the actual process, both situations are not conducive to the thermal safety of the process and design. In high cooling efficiency, heat removal can effectively (Q_{r1}) control heat generation to prevent runaway reaction to occur; however, if the size of the device is enlarged, the cost of the cooling system may be too high. At low cooling efficiency (Q_{r3}), heat removal is less than heat generation throughout the within process and does not reduce the possibility of a thermal runaway.

We recommend that the benefits of the cooling system fall within this range in $0.0213 < hS < 2.2027$ kJ min^{-1} K^{-1}, and assume moderate cooling efficiency (Q_{r3}). Three intersection points can be attained with Q_{r2} and Q_g, which are expressed as $T_{S,L}$, T_M, and $T_{S,H}$, and they represent the stable temperatures at low, medium and high surrounding temperatures, respectively. As indicated in curve Q_{r2}, it is difficult to maintain the temperature balance at T_M, as only a slight temperature fluctuation will break the thermal equilibrium which is conserved at T_M. It will no longer revert back to T_M when temperature changes, but will finish at either the lowest or the highest temperature at $T_{S,L}$ or

$T_{S,H}$, respectively. Therefore, how to define the required heat removal efficiency and keep the temperature in the system below the critical temperature is an important basis for maintaining the thermal safety characteristics of the real process.

Conclusions

For establishing additional thermokinetic parameters of DCBP 50.0 mass%, we applied curve fitting, isoconversional simulation, and a criticality approach to elucidate the decomposition reaction. The DSC tests results showed that DCBP released exothermic high heat under high-temperature conditions. Therefore, DCBP should be carefully stored and caution must be taken not to mix with incompatible material by accident, such as HNO_3 or other acid and alkaline materials.

References

1. Research and Markets. Global and Chinese di(2,4-Dichlorobenzoyl)peroxide (CAS 133-14-2) industry–2017. 2017. https://www.researchandmarkets.com/reports/4264860/. Accessed 20 Jan 2018.
2. Sheldon RA. Organic peroxygen chemistry. England: John Wiley & Sons, Inc.; 1992.
3. Amit B, James WR, Paramita R. Polymer grafting and crosslinking. England: John Wiley & Sons Inc.; 2009.
4. Czech Z, Goracy K. Characterization of crosslinking process of silicone pressure-sensitive adhesives. Polymer. 2005;50:762–4.
5. Lee MH, Chen JR, Shiue GY, Lin YF, Shu CM. Simulation approach to benzoyl peroxide decomposition kinetic by thermal calorimetric technique. J Taiwan Inst Chem Eng. 2014;45:115–20.
6. Liu SH, Hou HY, Chen JW, Weng SY, Lin YC, Shu CM. Effects of thermal runaway hazard for three organic peroxides conducted by acids and alkalines with DSC, VSP2, and TAM III. Thermochim Acta. 2013;566:226–32.
7. Hou HY, Shu CM, Tsai TL. Reaction of cumene hydroxide mixed with sodium hydroxide. J Hazard Mater. 2008;152:1214–9.
8. US Department of Transportation. 2018. http://www.transportation.gov. Accessed 20 Jan 2018.
9. Semenov NN. The calculation of critical temperatures of thermal explosion. Z Phys Chem. 1928;48:571–2.
10. Dorn M. Environmental aspects of initiators for plastic manufacture and processing. The handbook of environmental chemistry, vol. 12. Berlin: Springer; 2010.
11. Aceox® Chemical Corp. 2018. http://www.acechem.com.tw. Accessed 20 Jan 2018.
12. UN Economic Commission for Europe. Globally harmonized system. 2018. https://www.unece.org/trans/danger/publi/ghs/ghs_rev07/07files_e0.html#c61353. Accessed 20 Jan 2018.
13. Tsai LC, You ML, Ding MF, Shu CM. Thermal hazard evaluation of lauroyl peroxide mixed with nitric acid. Molecules. 2012;17:8056–67.
14. Hsueh KH, Chen WC, Chen WT, Shu CM. Thermal decomposition analysis of 1,1-bis(*tert*-butylperoxy)cyclohexane with sulfuric acid contaminants. J Loss Prev Process Ind. 2016;40:357–64.
15. Hou HY, Liao TS, Duh YS, Shu CM. Thermal hazard studies for dicumly peroxide by DSC and TAM. J Therm Anal Calorim. 2006;1:167–71.
16. Li X, Koseki H, Iwata Y, Mok YS. Decomposition of methyl ketone peroxide and mixtures with sulfuric acid. J Loss Prev Process Ind. 2004;17:23–8.
17. Lin SY, Shu CM, Tsai YT, Chen WC, Hsueh KH. Thermal decomposition on Aceox BTBPC mixed withn hydrochloric acid. J Therm Anal Calorim. 2015;122:1177–89.
18. Cho YS, Shim MJ, Kim SW. Thermal degradation kinetic of PE by the Kissinger equation. Mater Chem Phys. 1998;52:94–7.
19. Sanchez PE, Criado JM, Perez LA. Kissinger kinetic analysis of data obtained under different heating schedules. J Therm Anal Calorim. 2008;94:427–32.
20. Blaine RL, Kissinger HE. Homer Kissinger and the Kissinger equation. Thermochim Acta. 2012;540:1–6.
21. Thitithammawong A, Sahakaro K, Noordermeer J. Effect of different types of peroxides on rheological, mechanical, and morphological properties of thermoplastic vulcanizes based on natural rubber/polypropylene blends. Polym Test. 2007;200(26):537–46.
22. Vyazovkin S. Model-free kinetics: staying free of multiplying entities without necessity. J Therm Anal Calorim. 2006;83:45–51.
23. Roduit B, Borgeat CH, Berger B, Folly P, Andres H, Schädeli U, Vogelsanger B. Up–scaling of DSC data of high energetic materials. J Therm Anal Calorim. 2006;85:195–202.
24. Vyazovkin S, Burnham AK, Criado JM, Pérez-Maqueda LA, Popescu C, Sbirrazzuoli N. The prediction of thermal stability of self-reactive chemicals. Thermochim Acta. 2011;520:1–19.
25. Sbirrazzuoli N, Vincent L, Mija A, Guigo N. Integral, differential and advanced isoconversional methods. Complex mechanisms and isothermal predicted conversion-time curves. Chemom Intell Lab Syst. 2009;96:219–26.
26. Galwey AK, Brown ME. A theoretical justification for the application of the Arrhenius equation to kinetics of solid state reactions (mainly ionic crystals). Proc R Soc Lond Ser A. 1995;450:501–12.
27. Vyazovkin S, Dollimore D. Linear and nonlinear procedures in isoconversional computations of the activation energy of non-isothermal reactions in solids. J Chem Inf Comput Sci. 1996;36:42–5.
28. Yuan MH, Shu CM, Kossoy AA. Kinetic and hazards of thermal decomposition of methyl ethyl ketone peroxide by DSC. Thermochim Acta. 2005;430:67–71.
29. ChemInform St. Petersburg, Ltd. 2018. http://www.cisp.spb.ru. Accessed 20 Jan 2018.
30. Product data sheet, Aceox® Chemical Corp. 2018. http://www.acechem.com.tw/products.asp?id=6&cat=1. Accessed 20 Jan 2018.
31. STARe Software with Solaris Operating System. Operating instructions. Switzerland: Mettler Toledo; 2017.
32. You ML, Hsieh TF. Thermal hazards evaluation on the manufacturing of LPO by DSC for environment protection in material engineering and its application. Adv Mater Res. 2012;600:75–9.
33. Lu KT, Yang CC, Lin PC. The criteria of critical runaway and stable temperatures of catalytic decomposition of hydrogen peroxide in the presence of hydrochloric acid. J Hazard Mater. 2006;135:319–27.
34. Lu KT, Luo KM, Lin SH, Su SH, Hu KH. The acid-catalyzed phenol–formaldehyde reaction: critical runaway conditions and stability criterion. Process Saf Environ Prot. 2004;82:37–47.